

Cite this: *Chem. Sci.*, 2020, **11**, 5289

All publication charges for this article have been paid for by the Royal Society of Chemistry

Received 16th March 2020  
Accepted 5th May 2020

DOI: 10.1039/d0sc01559h  
[rsc.li/chemical-science](http://rsc.li/chemical-science)

## Introduction

Non-covalent interactions are key forces that drive phenomena such as host–guest chemistry, molecular aggregation, crystallization and protein folding.<sup>1,2</sup> In recent years, important intermolecular interactions like hydrogen and halogen bonding<sup>3–7</sup> have been contextualized as  $\sigma$ -hole interactions.<sup>8–10</sup> A  $\sigma$ -hole can be seen as a Lewis acidic site along the vector of a covalent bond, the location of which coincides with the  $\sigma^*$  orbital of that bond. The extreme outcome of a  $\sigma$ -hole interaction can be the breaking and/or making of a  $\sigma$  bond, such as in the formation of  $I_3^-$  from molecular  $I_2$  and  $I^-$ .<sup>11,12</sup> A similar rationale can be applied to so-called ‘ $\pi$ -hole interactions’ involving electron-deficient aromatic rings,<sup>13,14</sup> or polarized double bonds with related covalent bond-forming chemistry such as in aldol-type reactions. In principle,  $\sigma$ - and  $\pi$ -hole interactions should be available with all the non-metallic elements of the periodic table. This includes carbon;<sup>15–17</sup> an element of central importance to life and ubiquitous presence in synthetic chemistry.

One might thus wonder to what extend carbon can be exploited as locus of Lewis acidity to establish ‘tetrel-bonding

## Observations of tetrel bonding between $sp^3$ -carbon and THF<sup>†</sup>

Victoria L. Heywood,<sup>b</sup> Thomas P. J. Alford,<sup>b</sup> Julius J. Roeleveld,<sup>a</sup> Siebe J. Lekanne Deprez,<sup>a</sup> Abraham Verhoofstad,<sup>a</sup> Jarl Ivar van der Vlugt,<sup>b</sup> Sérgio R. Domingos,<sup>b</sup> Melanie Schnell,<sup>b</sup> Anthony P. Davis<sup>b</sup> and Tiddo J. Mooibroek<sup>b</sup> <sup>\*a</sup>

We report the direct observation of tetrel bonding interactions between  $sp^3$ -carbons of the supramolecular synthon 3,3-dimethyl-tetracyanocyclopropane (**1**) and tetrahydrofuran in the gas and crystalline phase. The intermolecular contact is established via  $\sigma$ -holes and is driven mainly by electrostatic forces. The complex manifests distinct binding geometries when captured in the crystalline phase and in the gas phase. We elucidate these binding trends using complementary gas phase quantum chemical calculations and find a total binding energy of  $-11.2$  kcal mol<sup>-1</sup> for the adduct. Our observations pave the way for novel strategies to engineer  $sp^3$ -C centred non-covalent bonding schemes for supramolecular chemistry.

interactions’ (in analogy to halogen- and chalcogen-bonds).<sup>18</sup> Such interactions are well-known for  $sp^2$ -hybridized C-atoms in carbonyls<sup>19–26</sup> and have recently been reported for the  $sp$ -hybridized C-atoms of (coordinated) acetonitrile,<sup>27</sup> carbon monoxide<sup>28</sup> and carbon dioxide.<sup>29–32</sup> Non-covalent interactions with  $sp^3$ -hybridized carbon atoms are implicated in the advent of canonical  $S_N2$  nucleophilic displacement reactions<sup>12,33–35</sup> and can persist with methyl groups in crystal structures.<sup>36–38</sup>

However, a supramolecular synthon to predictably generate directional tetrel-bonding interactions centred on  $sp^3$ -C has not yet been experimentally disclosed. We envisaged that 1,1,2,2-tetracyanocyclopropane (TCCP) derivatives could fulfil this role.<sup>39,40</sup> These rings are synthetically viable and contain a sterically accessible electrophilic site located roughly on the two  $sp^3$  C-atoms in the  $(NC)_2C-C(CN)_2$  fragment. This is exemplified by the molecular electrostatic potential (MEP) map of 3,3-dimethyl-TCCP (**1**) shown in Fig. 1. The calculated  $\sigma$ -hole potential of  $+44$  kcal mol<sup>-1</sup> lies in-between the  $\sigma$ -holes of water ( $+55$  kcal mol<sup>-1</sup>) and ammonia ( $+35$  kcal mol<sup>-1</sup>), which are prototypical  $\sigma$ -hole (*i.e.* hydrogen bond) donors. The Lewis acidic site of **1** should thus be able to form a tetrel bonding interaction with an electron-rich partner such as the lone pair electron cloud on tetrahydrofuran (THF, estimated at  $-40$  kcal mol<sup>-1</sup>).<sup>39–41</sup> Here we report on the verification of this hypothesis by synthesizing **1** and showing that – as anticipated – **1** binds to THF *via* intermolecular  $sp^3$ -C $\cdots$ O interactions, both in the crystalline state and in the gas phase.

## Results and discussion

Cyclopropane **1** was readily prepared in a one-pot cascade reaction from acetone, malononitrile and molecular bromine (Scheme 1). Presumably, cyclization to **1** proceeds from an

<sup>a</sup>van 't Hoff Institute for Molecular Sciences, Universiteit van Amsterdam, Science Park 904, 1098 XH Amsterdam, The Netherlands. E-mail: [t.j.mooibroek@uva.nl](mailto:t.j.mooibroek@uva.nl)

<sup>b</sup>School of Chemistry, University of Bristol, Cantock's Close, Bristol, BS8 1TS, UK

<sup>†</sup>Institute of Chemistry, Carl von Ossietzky University Oldenburg, Carl-von-Ossietzky-Straße 9-11, D-2629 Oldenburg, Germany

<sup>‡</sup>Deutsches Elektronen-Synchrotron (DESY), Notkestraße 85, 22607 Hamburg, Germany

<sup>§</sup>Institut für Physikalische Chemie, Christian-Albrechts-Universität zu Kiel, Max-Eyth-Str. 1, 24118 Kiel, Germany

<sup>†</sup> Electronic supplementary information (ESI) available. CCDC 1983293. For ESI and crystallographic data in CIF or other electronic format see DOI: [10.1039/d0sc01559h](https://doi.org/10.1039/d0sc01559h)



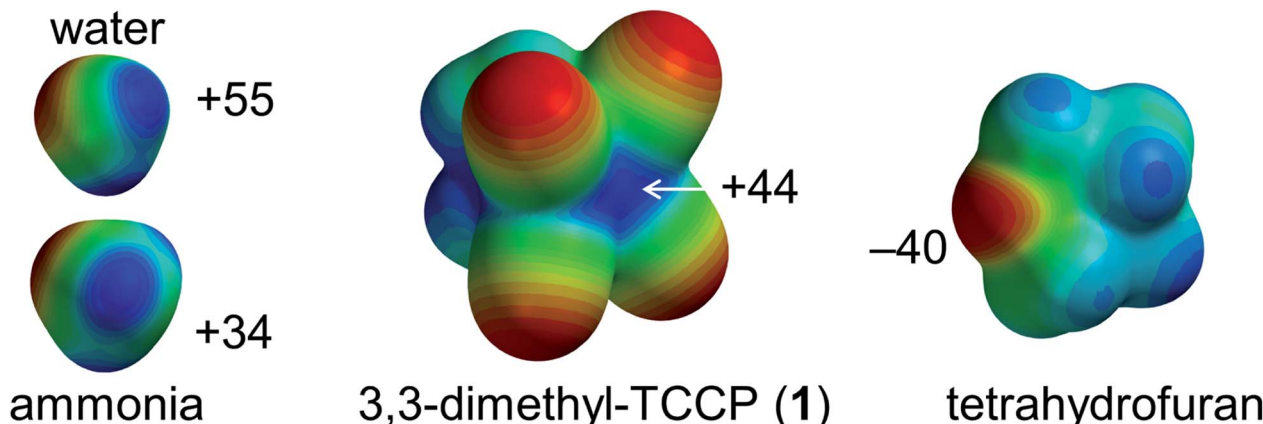


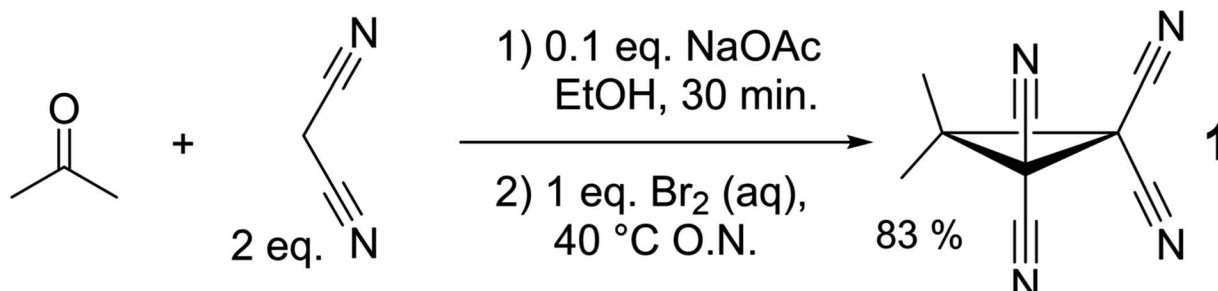
Fig. 1 Molecular Electrostatic Potential maps (MEP) of water, ammonia, 3,3-dimethyl-TCCP (1) and tetrahydrofuran (THF) calculated at the DFT/B3LYP-D3/def2-TZVP level of theory. The MEP is colour coded from electropositive (blue) to electronegative (red), and the indicated potentials are in  $\text{kcal mol}^{-1}$ .

intermediate formed by the nucleophilic attack of *in situ* generated  $[\text{BrC}(\text{CN})_2]^-$  on the Knoevenagel condensation product of acetone and malononitrile.<sup>42</sup> The yield of our procedure (83%) is higher than obtained by previously reported methods<sup>42-48</sup> (max. 72%).<sup>47</sup> All literature procedures with a yield in excess of 50%<sup>42,43,45-48</sup> (maximum 72%)<sup>47</sup> use a two-step approach starting from an activated malononitrile derivative<sup>42,43,45-47</sup> and/or use electrochemical synthesis.<sup>47,48</sup>

Single crystals suitable for X-ray diffraction measurements (see ESI† for details) were obtained by slow evaporation of a solution of **1** in THF. The molecular model of  $[\mathbf{1}\cdots\text{THF}]$  resulting from the diffraction study is shown in Fig. 2a. All the intramolecular distances and angles within this structure can be considered as normal (not shown).<sup>49</sup> The plane running through the O- and C-atoms of the THF molecule is roughly coplanar with the cyclopropane ring plane in **1** ( $\angle_{\text{plane-plane}} = 8.2^\circ$ ). Interestingly, the oxygen atom of the THF molecule is directed towards C1/C3/C4 of the cyclopropane ring in **1**, with very short intermolecular distances, in particular  $\text{sp}^3\text{-C1}\cdots\text{O1}$  of 3.007 Å (C3/C4  $\cdots$  O1 = 3.1 Å, not shown). This is 0.213 Å within the van der Waals radii of O (1.52 Å) and C (1.70 Å) and thus consistent with a bonding interaction.<sup>12,27,39,40,50</sup> Further stacking of  $[\mathbf{1}\cdots\text{THF}]$  in the crystal is aided by weak N1/N2 $\cdots$ C1/C3/C4 interactions (max. 0.067 Å van der Waals overlap, see Fig. S3†).‡

A DFT optimization at the B3LYP<sup>51,52</sup>-D3(BJ)<sup>53</sup>/def2-TZVP<sup>54,55</sup> level of theory of the atomic coordinates found in the crystal structure converged at a nearly identical structure (see Fig. S5†). The interaction energy ( $\Delta E$ ) was computed to be  $-10.1 \text{ kcal mol}^{-1}$ . This is much larger than interactions of dimethyl ether halogen bonded to  $\text{I-C}_6\text{F}_5$  ( $-5.6 \text{ kcal mol}^{-1}$ ) or hydrogen bonded to water ( $-6.7 \text{ kcal mol}^{-1}$ ) at this same level of theory.<sup>37,56</sup> Interestingly, the  $[\mathbf{1}\cdots\text{THF}]$  structure shown in Fig. 2b was found to be  $1.1 \text{ kcal mol}^{-1}$  more stable, representing the true energetic minimum with  $\Delta E = -11.2 \text{ kcal mol}^{-1}$  (see also Fig. S6†). The structure is similar to the crystal structure but with the THF oriented almost perpendicular to the cyclopropane plane, with  $\angle_{\text{plane-plane}} = 83.8^\circ$ . The distances between the THF-O and the two  $\text{sp}^3$   $(\text{NC})_2\text{C-C}(\text{CN})_2$  atoms display up to 0.297 Å van der Waals overlap, which is 0.084 Å more than observed in the crystal structure. This difference likely originates from the lack of any other interactions in the idealized gas phase computation *versus* various other potential weak interactions within the crystal of  $[\mathbf{1}\cdots\text{THF}]$ .

Rotational spectroscopy is the technique to experimentally discriminate between the two relative orientations of  $[\mathbf{1}\cdots\text{THF}]$  (Fig. 2) that are so close in energy in the gas phase calculations ( $1.1 \text{ kcal mol}^{-1}$ ). Thus, we conducted chirped pulse Fourier transform microwave (CP-FTMW) spectroscopy<sup>57,58</sup> to assign the geometry of  $[\mathbf{1}\cdots\text{THF}]$  in the gas phase (see ESI† for



Scheme 1 One-pot cascade synthesis of **1**.



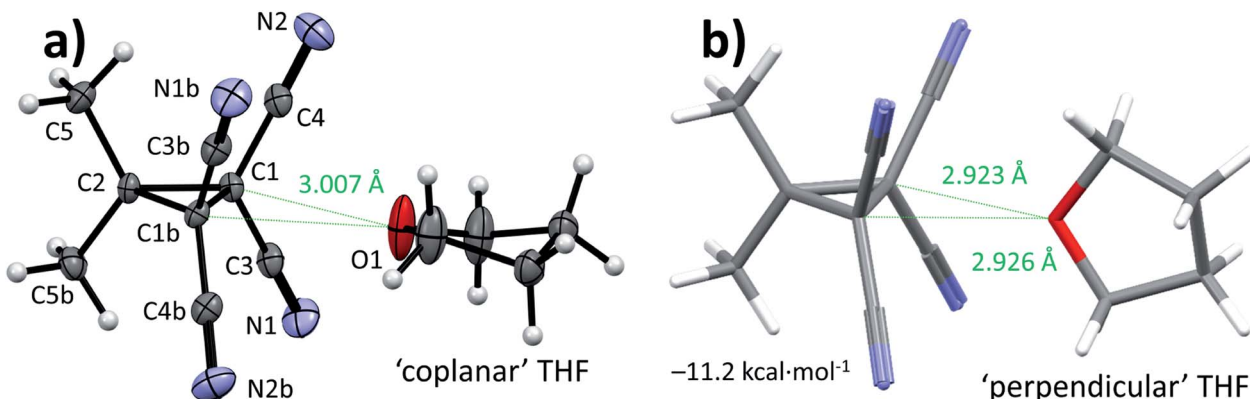


Fig. 2 (a) Single crystal X-ray diffraction structure of  $[1 \cdots \text{THF}]$  with heavy atoms represented as thermal ellipsoids drawn at 50% probability and hydrogen atoms drawn as spheres with 0.15 Å radius (the unit cell was expanded along a two-fold symmetry axis running through  $\text{C}2$  and  $\text{O}1$ ). (b) Capped sticks representation of the energy minimum ( $\Delta E = -11.2 \text{ kcal mol}^{-1}$ ) of  $[1 \cdots \text{THF}]$  found by DFT (B3LYP-D3(BJ)/def2-TZVP) and consistent with gas phase microwave spectroscopy data. Carbon = grey, nitrogen = blue, oxygen = red and hydrogen = white.

Table 1 Rotational constants  $A$ ,  $B$ ,  $C$ , quartic centrifugal distortion constant  $D_J$ , and dipole moment components  $\mu_i$ , for  $[1 \cdots \text{THF}]$  obtained from high resolution rotational spectroscopy and compared to values predicted with DFT<sup>a</sup>

	Experiment <sup>b</sup>	DFT <sup>c</sup>	
		Coplanar	Perpendicular
$A/\text{MHz}$	632.927(43)	633.88	635.59
$B/\text{MHz}$	342.56932(93)	326.09	341.81
$C/\text{MHz}$	316.7863(10)	325.50	317.89
$D_J/\text{kHz}$	0.0135(35)	—	—
$ \mu_a /D$	Observed	2.6	2.6
$ \mu_b /D$	Not observed	0.0	0.0
$ \mu_c /D$	Not observed	0.0	0.0
$N^d$	46	—	—
$\sigma/\text{kHz}^e$	22.1	—	—
$\Delta E \text{ (kcal mol}^{-1}\text{)}^c$	—	+1.1	0

<sup>a</sup> For the purpose of structure determination of the  $[1 \cdots \text{THF}]$  adduct in the gas phase, the hyperfine structure observed in the rotational spectrum has not been fitted entirely and only centre frequencies are used for the reported fit. As such the quadrupole coupling constants for the four nitrogen nuclei are not reported at this moment. This second layer of analysis of the spectrum goes beyond the scope of this work and will be reported later in a separate manuscript. <sup>b</sup> The errors for the measured values are standard errors. The experimental frequency accuracy is 25 kHz. <sup>c</sup> The predicted rotational constants were obtained from a DFT calculation at the B3LYP-D3(BJ)/def2-TZVP level of theory. 'Coplanar' and 'perpendicular' refer to the orientation of the THF ring relative to the cyclopropane ring in **1** (see also Fig. 1).

<sup>d</sup> Number of lines included in the fit. <sup>e</sup> Standard deviation of the fit.

details). Shown in Table 1 are spectroscopic parameters extracted from this experiment together with predicted values based on DFT calculations of  $[1 \cdots \text{THF}]$  with 'coplanar' or 'perpendicular' THF orientations. The experimental rotational constants (in particular  $B$  and  $C$ ) provide a conclusive assignment of the  $[1 \cdots \text{THF}]$  complex in the 'perpendicular' orientation, which is also the DFT-energetic minimum (right-hand side of Fig. 2).

To date we were unable to quantify tetrel bonding interactions with **1** in solution, but we did observe a very large and

unusual solvent dependency for the  $^1\text{H}$  and  $^{13}\text{C}$  NMR resonances of **1** (detailed in Fig. S7 and Table S4<sup>†</sup>). For example, the methyl protons of **1**, which are  $\gamma$  to CN, span a range of 1.39 ppm passing from benzene through toluene, acetonitrile, methanol and chloroform, to acetone. In comparison, the ethoxy methyl protons in ethyl acetate and diethyl ether vary by just 0.34 and 0.12 ppm, despite being closer to functional groups.<sup>64</sup> These results seem to suggest strong and geometrically specific interactions between **1** and most solvent molecules. Based on these preliminary observations, we anticipate that future studies will demonstrate that tetrel bonding interactions with tetracyanocyclopropane derivatives also persist in solution.

To gain more insight into the physical origins of the  $[1 \cdots \text{THF}]$  adduct, the 'perpendicular' structure was subjected to a Morokuma-Ziegler inspired energy decomposition,<sup>37,59–61</sup> an 'atoms-in-molecules',<sup>62</sup> and a non-covalent interaction analysis.<sup>63</sup> The energy decomposition analysis revealed that the interaction is mainly electrostatic in origin (52.7%) followed by dispersion (30.7%) and orbital interactions (16.8%). Interestingly, orbital mixing occurred between the HOMO of THF and the LUMO of **1** ( $-3.86 \text{ kcal mol}^{-1}$  stabilization) and between the HOMO-1 of THF and the HOMO of **1** ( $-4.80 \text{ kcal mol}^{-1}$  stabilization, see Fig. S8<sup>†</sup> for details). The 'atoms-in-molecules' analysis of  $[1 \cdots \text{THF}]$  shown in Fig. 3a reveals several bond critical points (bcps) between the N-atoms of **1** and several CH hydrogens of THF, indicating very weak hydrogen bonding interactions ( $\rho \approx 0.005 \text{ a.u.}$ ). The densest bcp of  $\rho = 0.0115 \text{ a.u.}$  is present between the THF O-atom and one of the  $\text{sp}^3$   $(\text{NC})_2\text{C-C}(\text{CN})_2$  atoms (highlighted in yellow).<sup>§</sup> In line with these results, the NCI plot shown in Fig. 3b clearly reveals that there are two  $\text{sp}^3\text{-C} \cdots \text{O}$  interactions that are mainly electrostatic in origin (blue), and that the C-H  $\cdots$  N interactions are mainly dispersive (yellow/green).

For comparison purposes, a cyclopentane adduct was calculated after *in silico*  $\text{O} \rightarrow \text{CH}_2$  mutation and geometry optimization of structure  $[1 \cdots \text{THF}]$ . This resulted in the structurally similar  $[1 \cdots \text{cyclopentane}]$  adduct shown in Fig. 3c (see



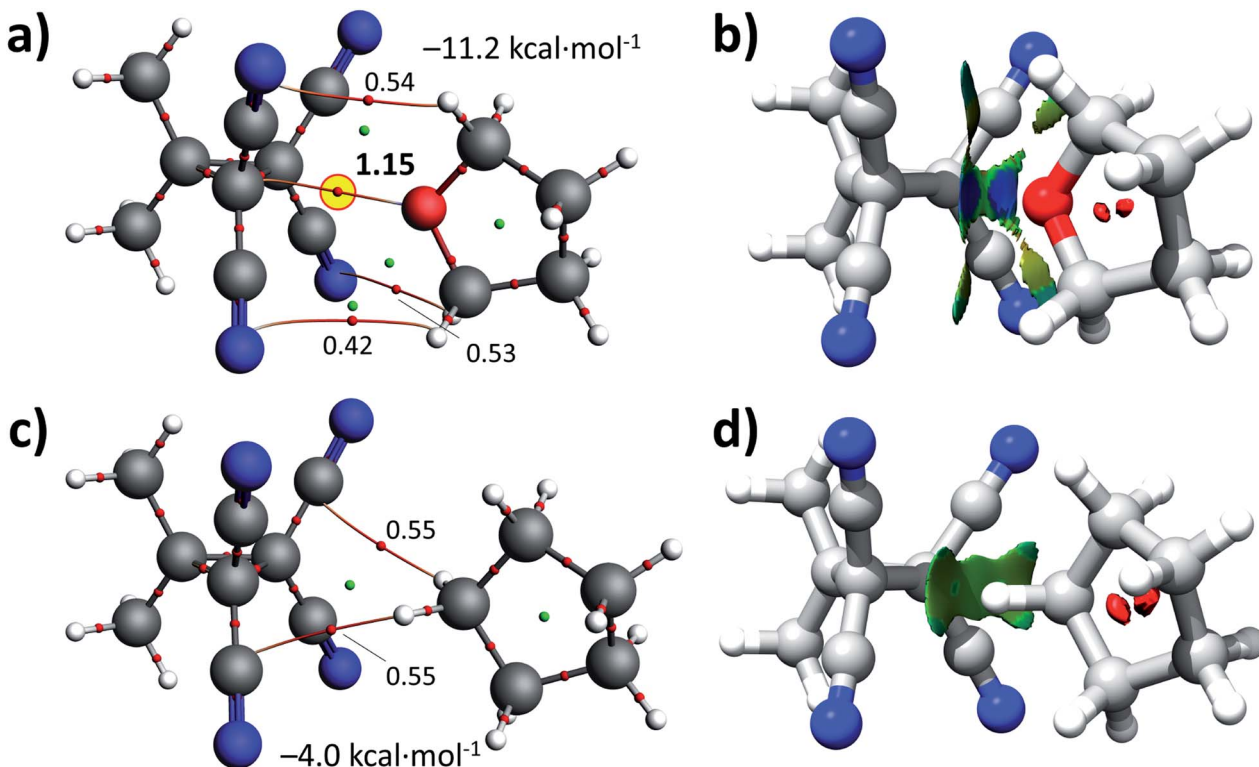


Fig. 3 Geometry optimized structures (B3LYP-D3/def2-TZVP) and ‘atoms-in-molecules’ analysis of [1···THF] (a, see also Fig. 2) and [1···cyclopentane] (c, obtained after *in silico* O → CH<sub>2</sub> mutation and optimization). The bond densities of the intermolecular bond critical points are represented by small red spheres ( $\rho$  in a.u.  $\times 100$ ). (b) and (d) show a non-covalent interactions (NCI) analysis using NCIPLLOT. Isosurface = 0.3 and regions in blue are mainly electrostatic interactions, in green are van der Waals dispersive forces and repulsions are in red.

also Fig. S9†). The ‘atoms-in-molecules’ analysis of this adduct reveals only two C–H···C≡N bcp’s ( $\rho \approx 0.0055$  a.u.). The adduct is also much less stable with  $\Delta E = -4.0$  kcal mol<sup>-1</sup>, which is mainly driven by dispersion (59.4%) followed by electrostatic interactions (22.2%). The NCI analysis of this adduct depicted in Fig. 3d clearly shows that this adduct is only held by dispersive C–H···N interactions (green).

## Summary and concluding remarks

In summary, it was shown that **1** can form [1···THF] complexes in the crystalline state and in the gas phase with a calculated interaction energy of up to -11.2 kcal mol<sup>-1</sup>. These complexes are held together by strong polar interactions between the *de facto* Lewis acidic site in between the sp<sup>3</sup>-hybridized C-atoms of **1** and the Lewis basic THF-O. These results demonstrate that tetrel-bonding interactions with sp<sup>3</sup>-carbon centres can indeed be used to engineer supramolecular complexes, thus paving the way for their exploration in other molecular disciplines, *e.g.* supramolecular chemistry, crystal engineering and medicine.

## Conflicts of interest

The authors declare no conflict of interest.

## Acknowledgements

TJM thanks NWO (VIDI project 723.015.006) and the EPSRC (EP/I028501/1) for funding. MS acknowledges financial support by the Deutsche Forschungsgemeinschaft in the context of the priority program SPP1807 (SCHN1280/4-2).

## Notes and references

‡ Attempts to co-crystallize **1** with various *n*-butylammonium salts were unsuccessful. However, cryospray ionization high resolution mass spectrometry of solutions of **1** and various *n*-butylammonium salts (Cl<sup>-</sup>, Br<sup>-</sup>, NO<sub>3</sub><sup>-</sup>, PF<sub>6</sub><sup>-</sup>) in CH<sub>2</sub>Cl<sub>2</sub> unambiguously revealed the corresponding [M+anion]<sup>-</sup> ions (Fig. S4,† top). All four adducts were calculated to be energetically stable by about -13 to -24 kcal mol<sup>-1</sup> (Fig. S4,† bottom).

§ The bond path is actually directed in between the two sp<sup>3</sup> C-atoms and only steeply curves to one of the C-atoms nearby the atoms.

- 1 P. J. Cragg, *Supramolecular Chemistry: From Biological Inspiration to Biomedical Applications*, Springer, Dordrecht, 1 edn, 2010.
- 2 A. Bauza, T. J. Mooibroek and A. Frontera, *ChemPhysChem*, 2015, **16**, 2496–2517.
- 3 H. J. Schneider, *Supramolecular Systems in Biomedical Fields*, RSC Publishing, Cambridge, UK, 1 edn, 2013.
- 4 T. Steiner, *Angew. Chem., Int. Ed.*, 2002, **41**, 48–76.
- 5 P. Metrangolo, H. Neukirch, T. Pilati and G. Resnati, *Acc. Chem. Res.*, 2005, **38**, 386–395.



6 *Hydrogen Bonding: New Insights*, ed. S. J. Grabowski, Springer, Heidelberg, 2006.

7 M. R. Scholfield, C. M. Vander Zanden, M. Carter and P. S. Ho, *Protein Sci.*, 2013, **22**, 139–152.

8 P. Politzer, J. S. Murray and P. Lane, *Int. J. Quantum Chem.*, 2007, **107**, 3046–3052.

9 S. J. Grabowski, *Phys. Chem. Chem. Phys.*, 2013, **15**, 7249–7259.

10 S. Scheiner, *Acc. Chem. Res.*, 2013, **46**, 280–288.

11 R. H. Crabtree, *Chem. Soc. Rev.*, 2017, **46**, 1720–1729.

12 A. Bauza, T. J. Mooibroek and A. Frontera, *Chem. Rec.*, 2016, **16**, 473–487.

13 C. A. Hunter and J. K. M. Sanders, *J. Am. Chem. Soc.*, 1990, **112**, 5525–5534.

14 B. L. Schottel, H. T. Chifotides and K. R. Dunbar, *Chem. Soc. Rev.*, 2008, **37**, 68–83.

15 S. J. Grabowski, *Chem.-Eur. J.*, 2013, **19**, 14600–14611.

16 J. S. Murray, P. Lane and P. Politzer, *J. Mol. Model.*, 2009, **15**, 723–729.

17 A. Bauza, T. J. Mooibroek and A. Frontera, *ChemPhysChem*, 2015, **16**, 2496–2517.

18 C. B. Aakeroy, D. L. Bryce, G. Desiraju, A. Frontera, A. C. Legon, F. Nicotra, K. Rissanen, S. Scheiner, G. Terraneo, P. Metrangolo and G. Resnati, *Pure Appl. Chem.*, 2019, **91**, 1889–1892.

19 P. Murrayrust, H. B. Burgi and J. D. Dunitz, *J. Am. Chem. Soc.*, 1975, **97**, 921–922.

20 H. B. Burgi, *Angew. Chem., Int. Ed.*, 1975, **14**, 460–473.

21 M. Harder, B. Kuhn and F. Diederich, *ChemMedChem*, 2013, **8**, 397–404.

22 G. J. Bartlett, A. Choudhary, R. T. Raines and D. N. Woolfson, *Nat. Chem. Biol.*, 2010, **6**, 615–620.

23 P. H. Maccallum, R. Poet and E. J. Milnerwhite, *J. Mol. Biol.*, 1995, **248**, 374–384.

24 A. Choudhary, D. Gandla, G. R. Krow and R. T. Raines, *J. Am. Chem. Soc.*, 2009, **131**, 7244–7246.

25 R. W. Newberry, G. J. Bartlett, B. VanVeller, D. N. Woolfson and R. T. Raines, *Protein Sci.*, 2014, **23**, 284–288.

26 E. C. Vik, P. Li, P. J. Pellechia and K. D. Shimizu, *J. Am. Chem. Soc.*, 2019, **141**, 16579–16583.

27 A. R. van der Werve, Y. R. van Dijk and T. J. Mooibroek, *Chem. Commun.*, 2018, **54**, 10742–10745.

28 M. T. Doppert, H. van Overeem and T. J. Mooibroek, *Chem. Commun.*, 2018, **54**, 12049–12052.

29 Y. P. Zeng, S. W. Sharpe, S. K. Shin, C. Wittig and R. A. Beaudet, *J. Chem. Phys.*, 1992, **97**, 5392–5402.

30 A. C. Legon, *Phys. Chem. Chem. Phys.*, 2017, **19**, 14884–14896.

31 S. Gao, D. A. Obenchain, J. C. Lei, G. Feng, S. Herbers, Q. Gou and J. U. Grabow, *Phys. Chem. Chem. Phys.*, 2019, **21**, 7016–7020.

32 M. Juanes, R. T. Saragi, W. Caminati and A. Lesarri, *Chem.-Eur. J.*, 2019, **25**, 11402–11411.

33 J. Langer, S. Matejcik and E. Illenberger, *Phys. Chem. Chem. Phys.*, 2000, **2**, 1001–1005.

34 J. Mikosch, S. Trippel, C. Eichhorn, R. Otto, U. Lourderaj, J. X. Zhang, W. L. Hase, M. Weidemuller and R. Wester, *Science*, 2008, **319**, 183–186.

35 S. Pierrefixe, J. Poater, C. Im and F. M. Bickelhaupt, *Chem.-Eur. J.*, 2008, **14**, 6901–6911.

36 V. R. Mundlapati, D. K. Sahoo, S. Bhaumik, S. Jena, A. Chandrakar and H. S. Biswal, *Angew. Chem., Int. Ed.*, 2018, **57**, 16496–16500.

37 T. J. Mooibroek, *Molecules*, 2019, **24**, 3370.

38 J. Dutta, D. Kumar Sahoo, S. Jena, K. D. Tulsiyan and H. S. Biswal, *Phys. Chem. Chem. Phys.*, 2020, **22**, 8988–8997.

39 A. Bauza, A. Frontera and T. J. Mooibroek, *Phys. Chem. Chem. Phys.*, 2016, **18**, 1693–1698.

40 A. Bauza, T. J. Mooibroek and A. Frontera, *Chem.-Eur. J.*, 2014, **20**, 10245–10248.

41 A. Bauza, T. J. Mooibroek and A. Frontera, *Phys. Chem. Chem. Phys.*, 2014, **16**, 19192–19197.

42 A. N. Vereshchagin, M. N. Elinson, N. O. Stepanov and G. I. Nikishin, *Mendeleev Commun.*, 2009, **19**, 324–325.

43 R. Huisgen and G. Mloston, *Heterocycles*, 1990, **30**, 737–740.

44 K. Kouno and Y. Ueda, *Chem. Pharm. Bull.*, 1985, **33**, 3998–4001.

45 H. Hart and Y. C. Kim, *J. Org. Chem.*, 1966, **31**, 2784–2789.

46 R. Huisgen, G. Mloston and E. Langhals, *Helv. Chim. Acta*, 2001, **84**, 1805–1820.

47 M. N. Elinson, S. K. Feducovich, T. L. Lizunova and G. I. Nikishin, *Tetrahedron*, 2000, **56**, 3063–3069.

48 G. I. Nikishin, M. N. Elinson, T. L. Lizunova and B. I. Ugrak, *Tetrahedron Lett.*, 1991, **32**, 2655–2656.

49 F. H. Allen, O. Kennard, D. G. Watson, L. Brammer, A. G. Orpen and R. Taylor, *J. Chem. Soc., Perkin Trans. 2*, 1987, S1–S19.

50 A. Bondi, *J. Phys. Chem.*, 1964, **68**, 441–452.

51 A. D. Becke, *Phys. Rev. A*, 1988, **38**, 3098–3100.

52 C. T. Lee, W. T. Yang and R. G. Parr, *Phys. Rev. B: Condens. Matter Mater. Phys.*, 1988, **37**, 785–789.

53 S. Grimme, J. Antony, S. Ehrlich and H. Krieg, *J. Chem. Phys.*, 2010, **132**, 154104.

54 F. Weigend and R. Ahlrichs, *Phys. Chem. Chem. Phys.*, 2005, **7**, 3297–3305.

55 F. Weigend, *Phys. Chem. Chem. Phys.*, 2006, **8**, 1057–1065.

56 J. M. Hoffmann, A. K. Sadhoe and T. J. Mooibroek, *Synthesis*, 2020, **52**, 521–528.

57 G. G. Brown, B. C. Dian, K. O. Douglass, S. M. Geyer, S. T. Shipman and B. H. Pate, *Rev. Sci. Instrum.*, 2008, **79**, 053103.

58 S. R. Domingos, K. Martin, N. Avarvari and M. Schnell, *Angew. Chem., Int. Ed.*, 2019, **58**, 11257–11261.

59 G. te Velde, F. M. Bickelhaupt, E. J. Baerends, C. F. Guerra, S. J. A. van Gisbergen, J. G. Snijders and T. Ziegler, *J. Comput. Chem.*, 2001, **22**, 931–967.

60 F. M. Bickelhaupt and E. J. Baerends, in *Reviews in Computational Chemistry, Vol 15*, ed. K. B. Lipkowitz and D. B. Boyd, Wiley-Vch, Inc, New York, 2000, vol. 15, pp. 1–86.

61 S. C. C. van der Lubbe and C. F. Guerra, *Chem.-Asian J.*, 2019, **14**, 2760–2769.

62 R. F. W. Bader, *Acc. Chem. Res.*, 1985, **18**, 9–15.

63 J. Contreras-Garcia, E. R. Johnson, S. Keinan, R. Chaudret, J. P. Piquemal, D. N. Beratan and W. T. Yang, *J. Chem. Theory Comput.*, 2011, **7**, 625–632.

64 G. R. Fulmer, A. J. M. Miller, N. H. Sherden, H. E. Gottlieb, A. Nudelman, B. M. Stoltz, J. E. Bercaw and K. I. Goldberg, *Organometallics*, 2010, **29**, 2176–2179.

